12 August 1999

International weekly journal of science

nature

£5.45 €7.99 FFr51 DM15 Lire 15000 A$16.50

www.nature.com

Enumerating crystal networks

Disease resistance
Plants avoid an 'arms race'

B-cell development
RAG revisited

Microearthquakes
Banding together

7. Madey, T. E., Yakshinskiy, B. V., Ageev, V. N. & Johnson, R. E. Desorption of alkali atoms and ions from oxide surfaces: Relevance to origins of Na and K in atmospheres of Mercury and the Moon. *J. Geophys. Res.* **103,** 5873–5887 (1998).
8. Sprague, A. L. *et al.* Distribution and abundance of sodium in Mercury's atmosphere, 1985–1988. *Icarus* **129,** 506–527 (1997).
9. Ip, W. The sodium exosphere and magnetosphere of Mercury. *Geophys. Res. Lett.* **13,** 423–426 (1986).
10. Mendillo, M. & Baumgardner, J. Constraints on the origin of the Moon's atmosphere from observations during a lunar eclipse. *Nature* **377,** 404–406 (1995).
11. Hunten, D. M. & Sprague, A. L. Origin and character of the lunar and Mercurian atmospheres. *Adv. Space Res.* **19,** 1551–1560 (1997).
12. Sprague, A. L., Kozlowski, R. W. H. & Hunten, D. M. Caloris Basin: An enhanced source for potassium in Mercury's atmosphere. *Science* **249,** 1140–1143 (1990).
13. Sprague, A. L., Kozlowski, R. W. H., Hunten, D. M., Wells, W. K. & Grosse, F. A. The sodium and potassium atmosphere of the Moon and its interaction with the surface. *Icarus* **96,** 7–42 (1992).
14. Mendillo, M., Emery, J. & Flynn, B. Modeling the Moon's extended sodium cloud as a tool for investigating sources of transient atmospheres. *Adv. Space Res.* **19,** 1557–1560 (1997).
15. Maschhoff, B. L., Pan, J.-M. & Madey, T. E. Medium-energy backscattered electron diffraction studies of TiO_2(110): relation to surface structure. *Surf. Sci.* **259,** 190–206 (1991).
16. Xu, X. & Goodman, D. W. The preparation and characterization of ultra-thin silicon dioxide films on a Mo (110) surface. *Surf. Sci.* **282,** 323–332 (1993).
17. Knotek, M. L. in *Desorption Induced by Electronic Transitions* (eds. Talk, N. H., Traum, M. M., Tully, J. C. & Madey, T. E.) 139–155 (Springer Ser. in Chemical Physics, Vol. 24, Springer, Berlin, 1983).
18. Potter, A. E. Jr & Morgan, T. H. Variation of sodium on Mercury with solar radiation pressure. *Icarus* **71,** 472–477 (1987).
19. Kozlowski, R. W. H., Sprague, A. L. & Hunten, D. M. Observation of potassium in the tenuous lunar atmosphere. *Geophys. Res. Lett.* **17,** 2253–2256 (1990).
20. Flynn, B. & Mendillo, M. Simulations of the lunar sodium atmosphere. *J. Geophys. Res.* **100,** 23271–23278 (1995).
21. Hellsing, B., Chakarov, D. V., Österlund, L., Zhdanov, V. P. & Kasemo, B. Photoinduced desorption of potassium atoms from a two-dimensional overlayer on graphite. *J. Chem. Phys.* **106,** 982–1002 (1997).
22. Wilde, M., Beauport, I., Al-Shamery, K. & Freund, H.-J. Photoinduced processes on alkali covered surface: NO desorption from K/Cr_2O_3 (0001). *Surf. Sci.* **390,** 186–193 (1997).
23. Ageev, V. N., Kuznetsov, Yu. A., Yakshinskiy, B. V. Madey, T. E. Electron stimulated desorption of alkali metal ions and atoms: Local surface field relaxation. *Nucl. Instrum. Meth. Phys. Res. B* **101,** 69–72 (1995).
24. Ageev, V. N., Kuznetsov, Yu. A. & Madey, T. E. Electron-stimulated desorption of sodium atoms from an oxidized molybdenum surface. *Phys. Rev. B* **58,** 2248–2252 (1998).
25. Mendillo, M., Baumgardner, J. & Wilson, J. Observational test for the solar wind sputtering origin of the Moon's extended sodium atmosphere. *Icarus* **137,** 13–23 (1999).
26. Heath, D. F. & Thekaekara, M. P. in *The Solar Output and its Variation* (ed. White, O. R.) 193–212 (Colorado Assoc. Univ. Press, Boulder, 1977).
27. Kivelson, M. G. & Russel, C. T. *Introduction to Space Physics* 92 (Cambridge Univ. Press, 1995).
28. Zhou, X. L., Zhu, X. Y. & White, J. M. Photochemistry at adsorbate/metal interface. *Surf. Sci. Rep.* **13,** 73–220 (1991).
29. Verami, S., Barbieri, C., Benn, C. & Cremonese, G. Possible detection of meteor stream effects on the lunar sodium atmosphere. *Planet. Space Sci.* **46,** 1003–1006 (1998).

Acknowledgements. We thank R. E. Johnson, A. L. Sprague, D. M. Hunten, J. Kolodziej and V. N. Ageev for discussion and correspondence. This work was supported in part by the Planetary Atmospheres Division of NASA.

Correspondence and requests for materials should be addressed to T.E.M. (e-mail: madey@physics.rutgers.edu).

Systematic enumeration of crystalline networks

Olaf Delgado Friedrichs*, Andreas W. M. Dress*†, Daniel H. Huson‡, Jacek Klinowski§ & Alan L. Mackay‖

** FSP Mathematisierung-Strukturbildungsprozesse, Universität Bielefeld, D-33501 Bielefeld, Germany*
† Department of Chemical Engineering, City College, CUNY, Convent Avenue at 140th Street, New York, New York 10031, USA
‡ Department of Mathematics, Princeton University, Princeton, New Jersey 08544-1000, USA
§ Department of Chemistry, University of Cambridge, Lensfield Road, Cambridge CB2 1EW, UK
‖ Department of Crystallography, Birkbeck College (University of London), Malet Street, London WC1E 7HX, UK

The systematic enumeration of all possible networks of atoms in inorganic structures is of considerable interest. Of particular importance are the 4-connected networks (those in which each atom is connected to exactly four neighbours), which are relevant to a wide range of systems—crystalline elements, hydrates, covalently bonded crystals, silicates and many synthetic compounds. Systematic enumeration is especially desirable in the study of zeolites and related materials, of which there are now 121 recognized structural types[1], with several new types being identified every year. But as the number of possible 4-connected three-dimensional networks is infinite, and as there exists no systematic procedure for their derivation, the prediction of new structural types has hitherto relied on empirical methods (see, for example, refs 2–4). Here we report a partial solution to this problem, based on recent advances in mathematical tiling theory[5–8]. We establish that there are exactly 9, 117 and 926 topological types of, respectively, 4-connected uninodal, binodal and trinodal networks, derived from simple tilings based on tetrahedra. (Here nodality refers to the number of topologically distinct vertices from which the network is composed.) We also show that there are at least 145 more distinct uninodal networks based on a more complex tiling unit. Of the total number of networks that we have derived, only two contain neither three- nor four-membered rings, and most of the binodal and trinodal networks are new.

We define a tiling as a periodic subdivision of space into bounded, connected regions without holes, which we call tiles. If two tiles meet along a surface, we call the surface a face. If three or more faces meet along a curve, we call the curve an edge. Finally, if at least three edges meet at a point, we call that point a vertex. Vertices and edges together form a network. A network can be derived from a tiling whenever it is possible to choose a collection of simple cycles (closed circuits) such that each edge occurs in at least three of them, and the cycles can be spanned by non-intersecting faces such that the union of all faces separates space into tiles. We note the distinction between faces and rings (usually defined as cycles without short cuts[9]).

We have earlier solved the much simpler problem of classifying all periodic tilings of the euclidean plane, the sphere and the hyperbolic plane[7,10]. Our algorithms[10] enumerate, and permit the visualization of, all possible topological types of tilings for each two-dimensional symmetry group with 1, 2, 3 (and so on) kinds of inequivalent vertices. We shall call these uninodal, binodal, trinodal (and so on) tilings. This approach has been applied to the enumeration of polyoxometalate cages[11]. We can now address the three-dimensional case, which has direct applications to structural chemistry.

The starting point is to associate with each type of periodic tiling

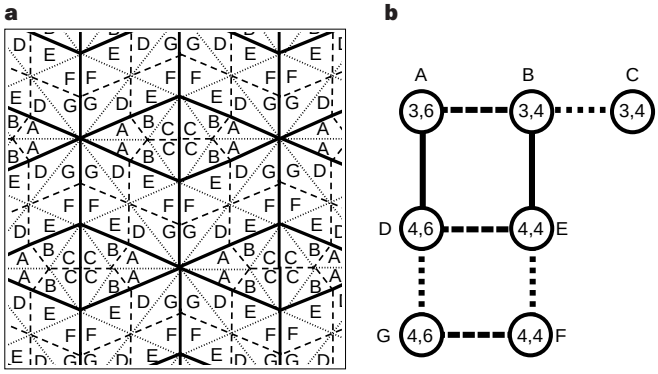

Figure 1 Derivation of the Delaney symbol for a tiling. **a**, The periodic tiling (bold lines) is barycentrically subdivided into triangles. Dotted lines join vertices to tile centres, and dashed lines join edge centres to tile centres. There are seven different classes of triangles, labelled A–G. **b**, Each class of triangle in **a** is represented by a node of the graph. The nodes are joined by lines corresponding to the edges of the triangles. For example, the nodes representing D and E are joined by a dashed line because the corresponding triangles have a dashed edge in common. In addition, each node is labelled by two numbers, the first indicating the number of edges of an original tile containing a triangle of the given class, the second indicating the degree of an original vertex belonging to a triangle of the given class (that is, the number of original edges meeting at this vertex). For example, node G is labelled '4,6' because a triangle of class G is contained in a four-sided tile and its original vertex is of degree 6. The designation A–G of the triangles is arbitrary, and the final Delaney symbol is unique for each kind of periodic tiling.

a unique "Delaney symbol"[6,7]. This is arrived at by breaking the tiling down into simplices using a barycentric subdivision. (Barycentric subdivision of a two-dimensional tiling is obtained by connecting the face centres to the vertices and edge centres: see Fig. 1a.) Any $n+1$ points in n-space which do not lie in an $(n-1)$ dimensional space are the vertices of an n-dimensional simplex. A simplex in two dimensions is thus a triangle, and in three dimensions a tetrahedron. In the two-dimensional case, the tiling is broken down into triangles (Fig. 1a), and each class of symmetrically equivalent triangles is then represented by a vertex of a graph. Whenever two triangles are adjacent, the corresponding vertices are joined by an edge. The Delaney symbol is obtained from the graph by appropriate labelling of vertices and 'colouring' of edges (Fig. 1b), and can alternatively be written as a string of characters, an 'inorganic gene'. The 'gene' for the tiling in Fig. 1 is

BAD36 ACE34 CBC34 EGA46 DFB44 GEF44 FDG46

where each group of characters contains information about one class of triangles in the barycentric subdivision: group 1 for class A, group 2 for class B, and so on. The letters refer to the neighbours across dashed, dotted and solid lines, respectively, of this class of triangles, while the numbers are the same as those inside circles in Fig. 1b.

The criteria by virtue of which the Delaney symbol encodes a tiling are as follows. (1) A given tiling translates to a linear sequence of characters, which can be put into a unique order by a rule, and vice versa. (2) This sequence is unique to the tiling. (3) There are rules to decide whether a sequence is 'legal', that is, corresponds to some actual tiling (see Supplementary Information). The classification of all periodic tilings of a given kind then reduces to the enumeration of the corresponding Delaney symbols, which is equivalent to 'mutating' the 'inorganic gene'. In principle, this approach can be used in any number of dimensions by dividing polytopal tiles into simplices.

In two dimensions, there are 11 different topological types of uninodal tilings, a result already known to Kepler[12], and 508 and 16,774 types of binodal and trinodal tilings, respectively[10]. By contrast, the number of types of uninodal tilings in three dimensions is infinite[13]. However, the number of possibilities becomes finite if we also limit the number of faces which can be incident to a common vertex or, alternatively, the number of faces which can be incident to a common tile (as well as the number of symmetrically inequivalent tiles). In the second case, the set of boundary faces of a given tile forms a two-dimensional tiling, which can be described by a two-dimensional Delaney symbol. The configuration of edges, faces and tiles around a fixed vertex can also be described by a two-dimensional Delaney symbol via the so-called vertex figure: place the centre of a small notational sphere at the vertex and consider the tiling of that sphere formed by the intersections with the different tiles touching that vertex. Some possible vertex figures for 4-connected networks are shown in Fig. 2.

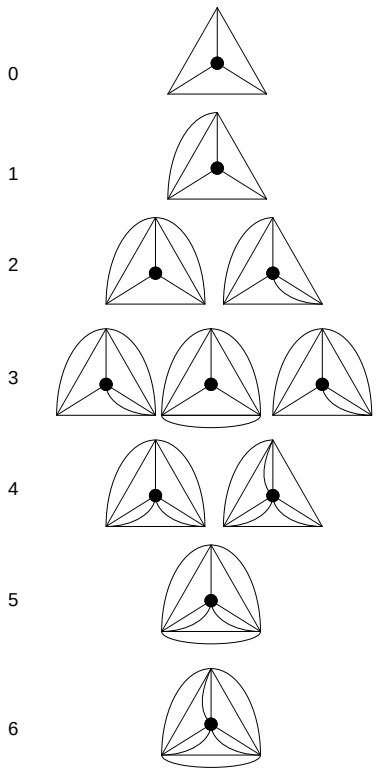

Figure 2 Vertex figures. The tetrahedral vertex figure with no extra edges (top) gives rise to 'simple' tilings; vertex figures with extra edges give 'quasi-simple' tilings. The number of extra edges is indicated on the left.

A specific vertex figure can be described in terms of a two-dimensional Delaney symbol (because it is a tiling of the sphere). To enumerate all possible tilings based on a given vertex figure, we must consider all possible 'three-dimensional' extensions of its two-dimensional symbol. The main difficulty is to determine which of the resulting three-dimensional symbols give rise to euclidean tilings (as opposed to tilings of, say, hyperbolic or spherical space). A practical solution has been found[14], by combining methods and results from group theory, topology and combinatorics.

Delaney symbols translate classification of tilings into purely algebraic problems. It only remains to develop and implement algorithms which solve them. Our computer program considers all possible 'legal' permutations of the 'gene', and then generates the corresponding tiling. We first enumerate all possible vertex figures of the desired kind, using our two-dimensional methods. Second, using advanced branch-and-bound techniques and the properties of crystallographic groups, we generate all possible three-dimensional extensions by generating all admissible face pairings and edge degrees for each feasible combination of vertex figures. Third, using methods from combinatorial group theory and topology, we determine whether such a tiling can be realized in three-dimensional euclidean space. Finally, if this is the case, we use optimization methods to construct a plausible realization of the actual tiling (see Supplementary Information).

Using this approach, we have been able to give a complete enumeration of all topological types of simple uninodal, binodal and trinodal tilings. The various networks generated in this way were compared with known structures using "coordination sequence" fingerprinting[15,16]. Thus in a 4-connected network, each vertex is connected to $N_1 = 4$ neighbouring vertices. These are linked to N_2 vertices in the next shell, in turn connected to N_3 vertices and so on, including each vertex only once. Although the coordination sequence for each kind of vertex is not unique to a given structure, it is a useful guide as structures with different coordination sequences must be different.

Simple tilings can give rise only to structures composed entirely of cages. We have considered those first, especially since networks with the lowest density tend to derive from simple tilings. We have established that there are nine possible topological types of simple uninodal tilings of euclidean space, each corresponding to a 4-connected network[17,18]. Six of them correspond to known zeolites (structure types SOD, LTA, RHO, FAU, KFI and CHA) and the remaining three have been described by O'Keeffe[3]. A systematic enumeration of all quasi-simple uninodal tilings yields 285 additional topological types. The total list of 294 tilings gives rise to at least 154 different 4-connected networks, among them the 12 remaining uninodal zeolites.

The enumeration of structure types with two or more symmetrically inequivalent types of tetrahedral vertices (binodal, trinodal, and so on) is addressed in a similar manner. We have established that there are exactly 117 and 926 topological types of simple

binodal and trinodal tilings of euclidean space, respectively. Some examples are shown in Fig. 3. Only two, corresponding to structure

chalcogenides and halides, to 3- and 4-connected carbon networks and to structures such as ice. Finally, bubbles found in foams are polyhedra in simple tilings. This means that every periodic foam with 1, 2 and 3 kinds of vertex will be found among our total of 1,052 (= 9 + 117 + 926) simple tilings. □

Received 18 May; accepted 28 June 1999.

1. Meier, W. M., Olson, D. H. & Baerlocher, C. *Atlas of Zeolite Structure Types* (Elsevier, London, 1996); updates available at ⟨http://www.iza-sc.ethz.ch/IZA-SC/Atlas/AtlasHome.html⟩.
2. Smith, J. V. Topochemistry of zeolites and related materials. 1. Topology and geometry. *Chem. Rev.* **88,** 149–182 (1988).
3. O'Keeffe, M. & Hyde, B. G. *Crystal Structures I: Patterns and Symmetry* (Monograph, Mineralogical Assoc. of America, Washington DC, 1996).
4. Treacy, M. M. J., Randall, K. H., Rao, S., Perry, J. A. & Chadi, D. J. Enumeration of periodic tetrahedral frameworks. *Z. Kristallogr.* **212,** 768–791 (1997).
5. Dress, A. W. M., Huson, D. H. & Molnár, E. The classification of face-transitive periodic 3-dimensional tilings. *Acta Crystallogr. A* **49,** 806–817 (1993).
6. Dress, A. W. M. in *Springer Lecture Notes In Mathematics* Vol. 1172, 56–72 (Springer, Göttingen, 1985).
7. Dress, A. W. M. Presentations of discrete groups, acting on simply connected manifolds, in terms of parametrized systems of Coxeter matrices: a systematic approach. *Adv. Math.* **63,** 196–212 (1987).
8. Huson, D. H. Combinatorial tiling theory: theorems-algorithms-visualization. At ⟨http://www.mathematik.uni-bielefeld.de/~delgado/Tiling-Theory⟩.
9. O'Keeffe, M. & Brese, N. E. Uninodal 4-connected 3D nets. I. Nets without 3-rings or 4-rings. *Acta Crystallogr. A* **48,** 663–669 (1992).
10. Huson, D. H. The generation and classification of tile-*k*-transitive tilings of the Euclidean plane, the sphere and the hyperbolic plane. *Geometriae Dedicata* **47,** 269–296 (1993).
11. Delgado Friedrichs, O., Dress, A. W. M., Müller, A. & Pope, M. T. Polyoxometalates: a class of compounds with remarkable topology. *Mol. Eng.* **3,** 9–28 (1993).
12. Kepler, J. *Harmonices Mundi Libri V* Book II, Sections 18–20, pp 51–56 (Linz, 1619).
13. Heesch, H. Über Raumteilungen. *Nachr. Gesellschaft Wiss. Göttingen* **1,** 35–42 (1934).
14. Delgado Friedrichs, O. Euclidicity criteria for three-dimensional branched triangulations. Thesis, Univ. Bielefeld (1994).
15. Brunner, G. O. & Laves, F. Zum Problem der Koordinazionszahl. *Wiss. Z. Tech. Univ. Dresden* **20,** 387–390 (1971).
16. Meier, W. M. & Moeck, H. J. The topology of three-dimensional 4-connected nets: classification of zeolite framework types using coordination sequences. *J. Solid State Chem.* **27,** 349–355 (1979).
17. Wells, A. F. *Three-Dimensional Nets and Polyhedra* (Wiley, New York, 1977).
18. Wells, A. F. *Further Studies of Three-Dimensional Nets* (Am. Crystallographic Assoc. Monogr. No. 8, Polycrystal Book Service, Pittsburgh, 1979).
19. Grünbaum, B. Uniform tilings of 3-space. *Geombinatorics* **4,** 49–56 (1994).
20. Gramlich-Meier, R. & Meier, W. M. Constituent units and framework conformations in zeolite networks. *J. Solid State Chem.* **44,** 41–49 (1982).

Supplementary information is available on *Nature*'s World-Wide Web site (http://www.nature.com) or as paper copy from the London editorial office of *Nature*.

Acknowledgements. We thank M. O'Keeffe for discussions.

Correspondence and requests for materials should be addressed to J.K. (e-mail: jk18@cam.ac.uk).

The mechanisms for pressure-induced amorphization of ice I_h

J. S. Tse*, D. D. Klug*, C. A. Tulk*, I. Swainson*, E. C. Svensson*, C.-K. Loong†, V. Shpakov‡, V. R. Belosludov‡, R. V. Belosludov§ & Y. Kawazoe§

* *Steacie Institute for Molecular Sciences, National Research Council of Canada, Ottawa, Ontario, Canada K1A 0R6*

† *Argonne National Laboratory, Argonne, Illinois 60439, USA*

‡ *Inorganic Chemistry Institute, Russian Academy of Sciences, Novosibirsk, Russia*

§ *Institute for Materials Research, Tokoku University, Sendai 980-8577, Japan*

There has been considerable interest in the structure of liquid water at low temperatures and high pressure following the discovery of the high-density amorphous (HDA) phase of ice I_h (ref. 1). HDA ice forms at a pressure close to the extrapolated melting curve of ice, leading to the suggestion that it may have structure similar to that of dense water. On annealing, HDA ice transforms into a low-density amorphous (LDA) phase with a distinct phase boundary[2,3]. Extrapolation of thermodynamic data along the HDA–LDA coexistence line into the liquid region has led to the hypothesis that there might exist a second critical point for water and the speculation that liquid water is mixture of two distinct structures with different densities[4,5]. Here we critically examine this hypothesis. We use quasi-harmonic lattice-dynamics calculations to show that the amorphization mechanism in ice I_h changes from thermodynamic melting for $T > 162$ K to mechanical melting at lower temperatures. The vibrational spectra of ice I_h, LDA ice and quenched water also indicate a structure for LDA ice that differs from that of the liquid. These results call into question the validity of there being a thermodynamic connection between the amorphous and liquid phases of water.

We used the quasi-harmonic lattice-dynamics[6] method to calculate the thermodynamic and mechanical stability boundaries of ice I_h under pressure. A thermodynamic solid–liquid stability boundary is determined by the equality of free energies of the two phases. In contrast, the mechanical stability boundary is obtained from purely mechanical stability conditions. To test for mechanical stability of the crystal, we calculated elastic constants at several pressures and temperatures. The maximum pressure of stability at a given temperature is determined *via* the Born stability criteria[7]. A mechanical instability in a solid occurs when particular combinations of the elastic constants violate one of the Born stability conditions[7]. Here we use a semi-empirical approach, combining the quasi-harmonic lattice dynamics and the Lindemann criterion for melting, to compute the thermodynamic melting line of ice I_h. This approach[8] has been applied successfully to a number of systems, including the correct description of the water–ice VI phase boundary. (For a recent application on related systems see refs 9, 10.)

The mechanical instability line due to the violation of the Born stability condition $C_{11} - |C_{12}| > 0$ (ref. 7) and the theoretical thermodynamic curves are compared with experiment in Fig. 1. The calculated thermodynamic melting curve agrees well with experiment[11] in the low-pressure/high-temperature region; the mechanical instability line agrees well with experiment in the high-pressure/low-temperature region. The temperature where mechanical instability occurs is always higher than the thermodynamic melting point. The most significant theoretical result is that the thermodynamic melting line meets the mechanical instability curve at ~160 K. This result, which agrees with experiment, shows that there are two distinct mechanisms for pressure-induced transformation of ice I_h in two different temperature regimes. This behaviour can be rationalized as follows. At high temperature, the water molecules have sufficiently large-amplitude thermal motions and consequently, the thermodynamic melting process takes precedence over mechanical instability. In contrast, at temperatures lower than 160 K the vibrational amplitudes of the water molecules are reduced, and the crystal structure collapses due to a mechanical instability under pressure.

In clathrate hydrates and their zeolite silica analogues, the mechanism for transformations to high-density amorphous phases at low temperatures has also been established to be a mechanical instability[12,13]. In contrast to ice I_h, the high-density phase made after pressurization in the clathrate hydrates of tetrahydrofuran (THF) and sulphur hexafluoride[12] could not be recovered even at 77 K. Instead, the transformed phase immediately reverted back to the initial crystalline solid. This reversible transformation would certainly not be feasible if the clathrate had actually undergone a melting transition to a quenched solution, as the formation kinetics of clathrate hydrate at 77 K are extremely slow[12]. This mechanism has been clearly demonstrated in a combined theoretical and experimental study of pressure-induced transformations in a THF zeolite[13].

Thermodynamic analysis of the extrapolated melting curve for ice I_h has shown[14] that the experimental results at high temperature and low pressure can be reproduced using reasonable parameters. However, this approach fails in the high-pressure/low-temperature region. For ice I_h the predicted amorphization pressure at 80 K of 6 kbar is substantially lower than the 11 kbar observed in experiments. A mechanical instability due to the softening of the elastic modulus C_{66} $(= C_{11} - C_{12})$ of the ice structure under high pressure has been proposed in a molecular dynamics study[15].